V. S. Frost
M. S. Perry
L. F. Dellwig
J. C. Holtzman
Remote Sensing Laboratory
University of Kansas Center for Research, Inc.
Lawrence, KS 66045

Digital Enhancement of SAR Imagery as an Aid in Geologic Data Extraction

Imagery processed by three methods (optically correlated, digitally correlated, and digitally enhanced) was evaluated.

Abstract: *Seasat-A synthetic-aperture radar (SAR) imagery taken over portions of the Southern Appalachians, correlated by optical and digital techniques and processed by a digital enhancement algorithm, was qualitatively evaluated for geologic data content in three phases to assess the relative amount of geologic data discernible. These phases included a lithologic analysis, a lineament analysis, and a geologic structural evaluation.*

The digital correlation process resulted in an image that appeared to be superior to the optically correlated image as a geological mapping tool. The digitally enhanced SAR images displayed marginally better correlation with the ground truth than did the corresponding digitally correlated images. More important, however, the enhancement program facilitated the interpretation of images. Mathematically, the enhancement algorithm is optimum in a mean square error sense, is computationally efficient, and tends to preserve the edge structure in SAR images because of its adaptive nature.

Introduction

Until 26 June 1978, all non-military active imaging radars employed conventional aircraft as system platforms. The launching of Seasat-A on that date marked the advent of orbital imaging radars. The imaging radar system included in the payload of Seasat-A was an L-band (23.5-cm wavelength) synthetic-aperture radar (SAR) that operated on an experimental basis until an electrical malfunction terminated operations on 9 October 1978. Both terrestrial and oceanic imagery was obtained over a number of areas before the malfunction occurred.

Data from the Seasat-A SAR have been routinely provided by the Jet Propulsion Laboratory in two formats resulting from two different methods of correlation. The standard technique employs an optical correlator which produces four strips of imagery for each 100-km swath the SAR sensed (Figure 1). The second method utilizes a digital correlation process that results in a single frame for each 100 by 100 kilometre square (Figure 2).

An apparent superiority of the digitally processed image as a data source prompts one to question whether or not such a format represents the optimum for data revelation, or if further processing might provide for more rapid and accurate data extraction or facilitate the extraction of additional data. Such processing may be discipline specific. A technique developed by Frost *et al.* (1981), which was designed to enhance Seasat-A digitally correlated images, was applied to an image of the Southern Appalachians and objectively evaluated for revelation of geologic data. Evaluation in-

Photogrammetric Engineering and Remote Sensing,
Vol. 49, No. 3, March 1983, pp. 357-364.

0099-1112/83/4903-0357$02.25/0

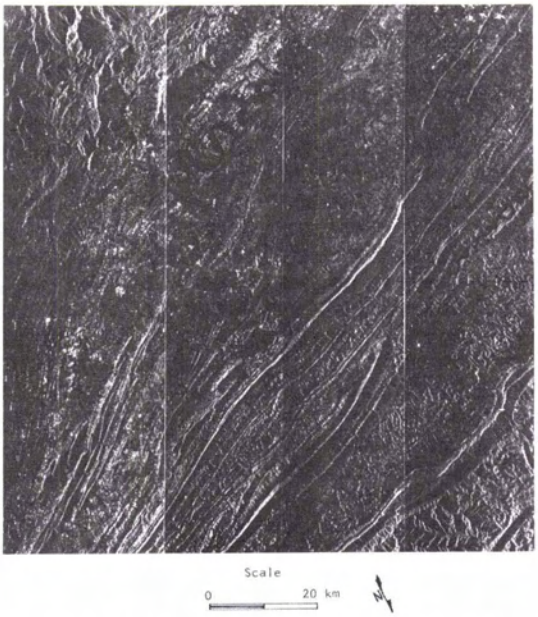

FIG. 1. Optically correlated Seasat-A image. Image orientation is dictated by look direction in this and all subsequent illustrations.

cluded an effort to separate as well as establish continuity of lithologies, to identify linear trends, and to interpret geologic structure. Documentation of relative value of each image was achieved only after correlation of Seasat-derived data with ground truth.

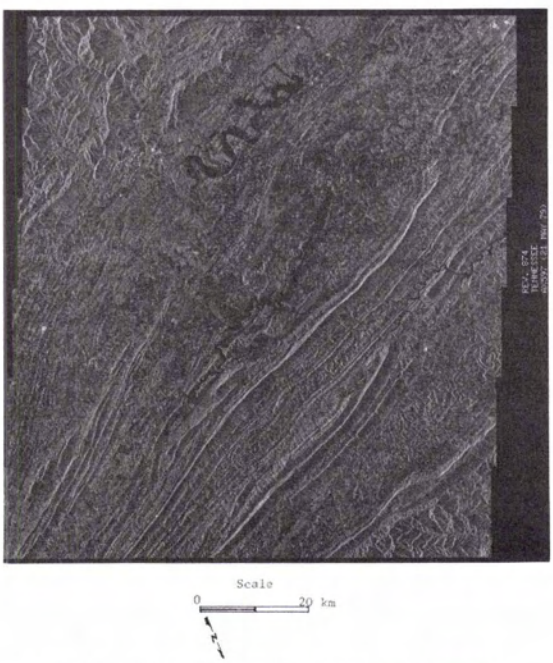

FIG. 2. Digitally correlated Seasat-A imagery.

SYNTHETIC APERTURE RADAR IMAGE FORMATION

The basic principles of SAR are well known (Kovaly, 1976; Harger, 1970; Jenson *et al.*, 1977). The purpose of this section is to briefly review the image formation for SAR and optical and digital SAR signal processing.

There are several different qualitative approaches to discussing SAR image formation, e.g., from a doppler frequency, antenna array theory, or matched filtering perspective. Here the SAR image formation process will be presented using antenna array theory. The azimuth resolution, ρ_a, of any radar is determined by the azimuth beamwidth, β, of its antenna and the range, R, to the target, i.e., $\rho_a = \beta R$. The beamwidth is in turn governed by the length, l, of antenna and the transmitting wavelength, λ, i.e., $\beta \approx \lambda/l$. Therefore, in order to improve the azimuth resolution, l must be increased (assuming fixed wavelength and range). However, the physical antenna length is limited by platform considerations and, if a spaceborne platform is to be used, then the range to scene is large.

These restrictions can be overcome by synthesizing a long antenna. This can be accomplished by treating the physical antenna for each transmitted pulse as an element of a much larger antenna array over some finite distance. To control the shape of the synthesized antenna array pattern, e.g., its beamwidth and mainlobe direction, the amplitude and phase weighting of each array element must be properly adjusted. That is, the received signal for each transmitted pulse must be properly adjusted in amplitude and phase to achieve the desired ρ_a which is independent of range and is suitable for the desired applications. Range resolution, ρ_r, is governed by the effective width in time, T, of the transmitted pulse, $\rho_r = cT/2$ (c = speed of light). A technique known as pulse compression is used to achieve the desired range resolution while reducing the peak power requirements. The image formation process must be designed to apply the proper amplitude and phase to the received signal for each transmitted pulse in order to synthesize the desired antenna characteristics. The received signal must also be processed in the range dimension to attain the desired range resolution. Note that the operations are defined for orthogonal dimensions, i.e., separate azimuth and range processing. Even though the concept of SAR is straightforward, its realization is complex. Because the purpose of this paper is to contrast the geologic mapping potential of SAR for one optical realization and one digital realization, the general operation of each process will be explained.

When optical processing is used to form SAR images, the received signal for each transmitted pulse (after coherent addition with a reference signal) is stored on photographic film as a vertical

line. Further, to record the bipolar signal on film it is necessary to add a bias to the signal prior to storage (Goodman, 1968). This photographic record is called the "SAR signal film." The spatial pattern of intensities on the signal film for a specific point in the terrain scene forms a Fresnel zone plate in the azimuth direction (Tomiyasu, 1978). That is, this spatial pattern has lense-like properties in the azimuth direction; thus, if illuminated with a coherent collimated light source, the signal film will focus the energy from a point to a point in azimuth. However, the focal length of this lens varies with the range to the target point so that a lens must be constructed which positions the focal points from any range on to the same plane. Further, the length of the synthesized antenna must be restricted, or equivalently the number of vertical range lines (pulses) to be processed as specified by the desired azimuth resolution. Note, if the azimuth resolution is to be independent of range, then the number of pulses processed also must vary with range. These two requirements can be simultaneously met by a conical lens. Focusing the return signal in the range direction is performed with a cylindrical lens. At this point both the range and azimuth information coincide on a plane but at infinity, i.e., the focal point of the azimuth and range processing is at infinity. Therefore, the final step is to use a spherical lens to form the radar image on the output film. Optical SAR processing relies on the propagation properties of coherent energy at visible wavelengths to perform the required amplitude and phase adjustments on the received signal.

When digital processing is used to form SAR images (Bennett and Cummings, 1979; Wu *et al.*, 1981), clearly the first step must be to convert the received variations in voltage into a sequence of numbers. This process is called analog-to-digital conversion. A separate sequence of numbers representing the received signal for each pulse, called a record, is stored on an appropriate computer storage medium, such as magnetic tape. A record is analogous to a vertical line stored on signal film. Because the original voltage (analog) was a bandpass signal, the data are stored in complex form, i.e., each sample has a real (in phase) and imaginary (quadrature) component and all numeric operations must operate on these complex data. Digital processing for SAR is a sequence of numerical operations designed to transform the collected records into a digital radar image. The first operation to be performed on the digitized records is pulse compression. As previously mentioned, some form of pulse coding is usually used to conserve transmitter power. Pulse compression can be viewed as linear filtering applied to each record. There are many ways of implementing the required digital filter (Oppenheim and Schafer, 1975). Such methods include discrete convolution which operates directly on the stored data, or Fast Fourier Transform (FFT) techniques which require a forward FFT to be applied to stored data, then complex multiply with the desired filter, and then inverse FFT. The two-dimensional output data from the pulse compression algorithm are then rotated 90° so that records are in the azimuth instead of the range direction in preparation for azimuth processing. Azimuth processing can also be viewed as a filtering operation; however, the characteristics of the filter change with range for reasons explained above. Filter characteristics for different range intervals are also stored in the digital processor. Azimuth filtering is performed using discrete convolution or FFT techniques. The output of the azimuth filtering operation is the radar image. This digital image is complex, i.e., for each scene coordinate a real and imaginary component is stored. A radar image for display can be produced from these complex numbers by transforming each complex value into its amplitude or power (the amplitude squared). The final digital radar image is thus formed and stored. A photograph for geologic interpretation can be generated from these data using standard techniques.

The above discussion of SAR image formation was general, and many details of both optical and digital processing were omitted. The purpose of this section was not to present the technical trade-offs between optical and digital SAR processing; rather, the intent was to introduce the basic concepts behind each technique in order to put the interpretation of digitally and optically generated SAR images in perspective.

Digital Image Enhancement for SAR

Imaging radars, specifically the synthetic-aperture radars (SAR), are beginning to make use of digital techniques, and digitally correlated SAR images are now becoming available. However, optimum techniques for enhancing digital radar images are not fully developed due to a lack of understanding of the properties of radar images from a digital image processing perspective.

A model-based image enhancement technique which was specifically designed for SAR images has been developed and implemented. This algorithm has been applied to digitally correlated Seasat-A SAR imagery of an area of geological interest. The purpose was to ascertain if this image enhancement algorithm improved the geologic mapping potential of the Seasat-A SAR. Before the results of this investigation are presented, the enhancement algorithms will be reviewed.

This enhancement algorithm was designed by first deriving a minimum mean square error (MMSE) filter to estimate the target reflectivity from the observed image. It was found that the parameters of MMSE filtering were a function of the target reflectivity mean and variance. To imple-

ment this filter, these parameters were estimated from the image and the characteristics of the filter were changed appropriately. An adaptive MMSE filter was thus constructed.

Summarizing the algorithm from Frost *et al.* (1981), an image of terrain can be viewed as being made up of many homogeneous areas. Each homogeneous area belongs to one of many terrain categories such as forests, urban areas, croplands, etc. The terrain reflectivity at each position within a homogeneous area can be modeled by a stationary random process $r(x,y)$. Fading, due to the coherent nature of the radar illumination, introduces a multiplicative noise component in the radar image (Goodman, 1976), and the point spread function of the imaging system further degrades the radar image. Thus, the recorded radar image $I(x,y)$ has the model Frost *et al.* (1980)

$$I(x,y) = [r(x,y)\cdot n(x,y)]*h(x,y) \tag{1}$$

where $n(x,y)$ is the multiplicative noise due to fading, $h(x,y)$ is the point spread function of the imaging system, and * denotes convolution. For SAR, $n(x,y)$ is modeled by a stationary, white, non-Gaussian random process with a χ^2 probability density function with $2N$ degrees of freedom, and N is the number of independent radar returns (looks) that were averaged.

The problem addressed here is one of processing the recorded image $I(x,y)$ in order to obtain an estimate of the reflectivity data $r(x,y)$, which we will call an ideal image. The impulse response $m(t)$, and the transfer function $M(f)$ of the minimum mean squared error (MMSE) filter that provides an estimate of $r(t)$ from $I(t)$ are obtained by minimizing the mean square error, ϵ, given by

$$\epsilon = E\{[r(t) - I(t)*m(t)]^2\} \tag{2}$$

$E\{\ \}$ denotes Expectation and $t = (x,y)$ is the spatial coordinate. The MMSE solution leads to a filter (Franks, 1969) with a transfer function

$$M(f) = \begin{cases} \left[\dfrac{\bar{n}S_r(f)}{S_r(f)*S_n(f)}\right]\dfrac{1}{H^*(f)} & \text{for } f \neq 0 \\ \dfrac{1}{\bar{n}} & \text{at } f = 0 \end{cases} \tag{3}$$

where $\bar{n} = E\{n(t)\}\cdot S_r(f)$ and $S_n(f)$ are the power spectral densities of the terrain reflectivity and the noise process, respectively. The filter given in Equation 3 is valid for smoothing SAR image data within homogeneous areas inside of which $r(t)$ can be modeled as a stationary random process. In Equation 3, $H^*(f)$ is the complex conjugate of the transfer function of the system which is not data dependent, and hence we will assume $H(f) = 1$ over some finite bandwith for purposes of illustrating the properties of the data dependent part of the filter $M'(f)$, i.e.,

$$M'(f) = \frac{\bar{n}S_r(f)}{S_r(f)*S_n(f)}\ . \tag{4}$$

A model for $r(t)$ is an auto-regressive process with an auto-correlation function (Habibi, 1972)

$$R_r(\tau) = \sigma_r^2\, e^{-a|\tau|} + \bar{r}^2 \tag{5}$$

where the parameters $\sigma_r^2, \bar{r}^2$ and 'a' have different values for different terrain categories. The model for the multiplicative white noise is

$$R_n(\tau) = \sigma_n^2\, \delta(t) + \bar{n}^2, \tag{6}$$

where $\delta(\tau)$ = delta function and the parameters σ_n^2 and $\bar{n}^2$ are sensor dependent but are not scene dependent. Substituting the power spectral densities of $r(t)$ and $n(t)$ in Equation 4, it can be shown that the impulse response of the filter is given by (Frost *et al.*, 1980)

$$m'(t) = K_1\, \alpha\, e^{-\alpha|t|} \tag{7}$$

with

$$\alpha = K_2\left(\frac{\sigma_I^2}{\bar{I}^2}\right) \tag{8}$$

where K_1 and K_2 are normalizing constants, and $\bar{I}$ and σ_I^2 are the mean and variance of the noisy input image $I(x,y)$. The constant, K_1, normalizes the filter impulse response so that the filter weights always sum to unity. The constant, K_2, is a function of N and, for the Seasat-A SAR, $K_2 \approx 12.8$. Thus, the only data dependent parameters needed to implement the filter are $\bar{I}^2$ and σ_I^2, which can be easily estimated from the image data.

To process the image at location (x_0,y_0), the parameters $\bar{I}^2$ and σ_I^2 are estimated using data from a local neighborhood (after experimentation, a 5 by 5 window was found to be best for Seasat-A SAR images) centered at (x_0,y_0), and the actual enhancement is done using the spatial domain version of the filter given in Equation 7. The filter actually performs a weighted averaging of data in the neighborhood of (x_0,y_0), the weights being determined from the local statistics of the data using Equations 7 and 8.

The algorithm is adaptive because the parameters are determined from the input data being scanned by the window. To illustrate how the algorithm handles boundaries, consider two homogeneous (stationary) areas A_1 and A_2 with $\bar{r}_1 = \bar{r}_2$ and $\sigma_{r_1}^2 > \sigma_{r_2}^2$. From Equation 8, it can be seen that $\alpha_1 > \alpha_2$, and hence from Equation 7 it follows that the impulse response of the MMSE filter is narrower in region A_1 than in A_2. Because $r(t)$ is the signal being estimated, if $r(t)$ has a larger variance, then a wide impulse response would excessively average the desired signal variations. Thus, for areas with large σ_r^2, the impulse response of the filter should be narrow and vice versa. Now, in the boundary region between A_1 and A_2, denoted by A_3, we have $\sigma_{r_3}^2 > \sigma_{r_1}^2$ and $\sigma_{r_2}^2$, and hence $\alpha_3 > \alpha_1$

and α_2. This implies that in a boundary area the impulse response has a very short duration, and hence very little averaging is done in the boundary areas. Thus, the adaptive algorithm preserves boundaries, whereas a non-adaptive filter would have blurred them. Further, this adaptive filter has been quantitatively and qualitatively shown to be superior to equal weighted and median filtering (Frost *et al.*, 1980). (For a complete description of the theoretical basis for the adaptive convolution, see Frost *et al.*, 1981.)

Test Area

Recognizing that any manipulation of raw data through processing or enhancement can be justified only on the basis of either providing an increased amount of information or facilitating greater ease of data extraction, a preliminary assessment of the value of these data manipulation techniques to the geologist was made. It was at the same time recognized that there are inherent drawbacks to a qualitative approach to evaluation, especially with a small group of analysts. However, even under such conditions, positive results should at least provide an impetus for continued research and development in processing techniques.

The test area consisted of approximately 10,000 square kilometres in the southern Appalachians (Figure 3), approximately two-thirds of which is included in the Valley and Ridge physiographic province of northeastern Tennessee and the remainder of which extends into the Cumberland Plateau Province of southern Virginia and Kentucky and the Blue Ridge Province of western North Carolina. This area was selected for study because of the excellent surficial expression of geologic structure.

Bedrock exposures are sparce, generally being covered by a regolith, the thickness of which is controlled by slope and underlying lithology (Harris and Kellberg, 1972). Exposures are limited to stream valleys, road cuts, quarries, and steep slopes with the amount of bedrock the SAR directly senses being essentially negligible (Ford, 1980).

FIG. 3. Study area.

Three areas were selected for enhancement (Figure 4). The Church Hill and Pine Mountain areas of enhancement are within the Valley and Ridge Province. The Cumberland Mountain area of enhancement bridges the Valley and Ridge Province and the adjacent Cumberland Plateau to the north, the separation in this area being parallel to the Kentucky-Virginia boundary. The Valley and Ridge Province is characterized by a subparallel, northwest-southeast alignment of ridges and valleys which have developed as a result of differential erosion of alternating competent and incompetent folded Paleozoic sedimentary rocks, whereas the Cumberland Plateau has suffered deep dissection but without pattern other than that imposed by erosion on essentially horizontal Carboniferous sedimentary rocks.

During the time of year that this imagery was obtained (summer of 1978), the slopes and ridges of the southern Appalachians were shrouded by a forest canopy of mixed coniferous and deciduous trees. Valleys were cultivated, grass covered, or forested. The geometry of the vegetative canopy generally reflects the underlying terrain (Ford, 1980).

Image Analysis

In order to compare the relative amount of geologic data discernible on orbital SAR imagery processed by the three methods, the three portions of the digitally correlated image were enhanced, imagery in the three formats was analyzed, and the data products were compared with one another and correlated with data revealed through field work.

The three enhanced areas were displayed on a cathode ray tube (CRT) and photographed with a 35-mm camera (Figures 5, 6, and 7). A telephoto lens was used to minimize the effects of the CRT screen curvature. An identical photographic procedure was used in recording the display of the corresponding three areas utilizing the computer compatible magnetic tape format of the digitally correlated image. Prints of the optically correlated image were generated at compatible scales from a duplicate negative.

All Seasat imagery analyzed was in a black-and-white positive print format at a range of scales, analysis being executed by visual means. Accuracy of feature definition as well as ease of data extraction was used to judge the potential of images generated by each processing technique for geologic mapping. Optically and digitally correlated images were analyzed at a scale of 1:245,000 and the enhanced images at a larger scale (1:91,000).

Each image was evaluated for isolation as well as continuity of lithologic units, revelation of line-

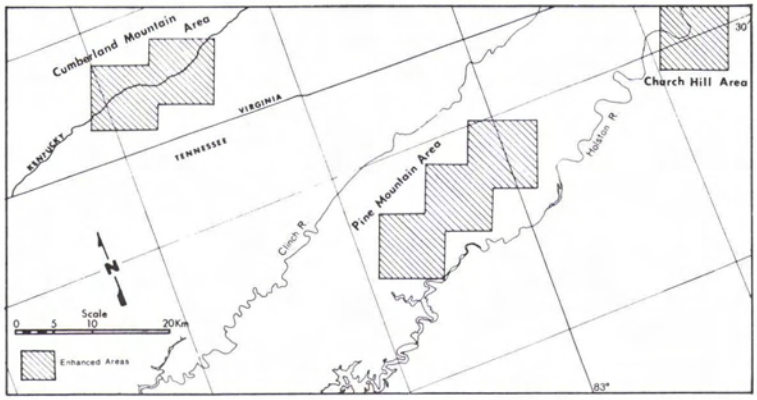

FIG. 4. Enhanced areas.

aments, and identification of geological structures. First, lithologic mapping was performed on all imagery, followed in turn by the lineament analysis and geological structure evaluation. In order to minimize prejudices, the sequence in which the imagery of the various correlation processes were evaluated was randomly altered. Relevant geologic maps or literature were not extensively consulted prior to image analysis. Subsequent to mapping, artifacts of cultural features were removed from the overlays of the enhanced areas through comparison with topographic sheets and aeronautical section maps, thus reducing the data content of the overlay to what was assumed to be surficial expressions of structural elements. During March 1980, a brief field check was performed in the research area which, along with data extracted from published sources (Rodgers, 1953; Hardeman *et al.*, 1966), provided a base for comparison with and evaluation of data derived from the imagery (Perry, 1980).

RESULTS

There were two factors considered in the comparison of the processing techniques: (a) The accuracy and consistency with which the geologic interpretation from imagery of each processing technique correlated with ground truth, and (b) a subjective quality, the ease of image interpretability.

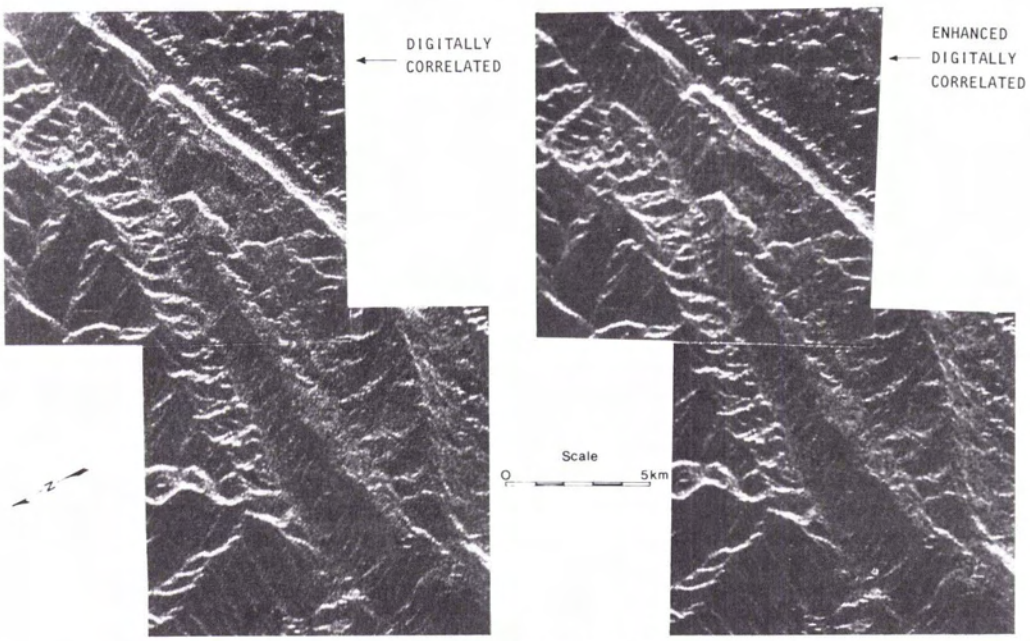

FIG. 5. Cumberland Mountain enhanced area.

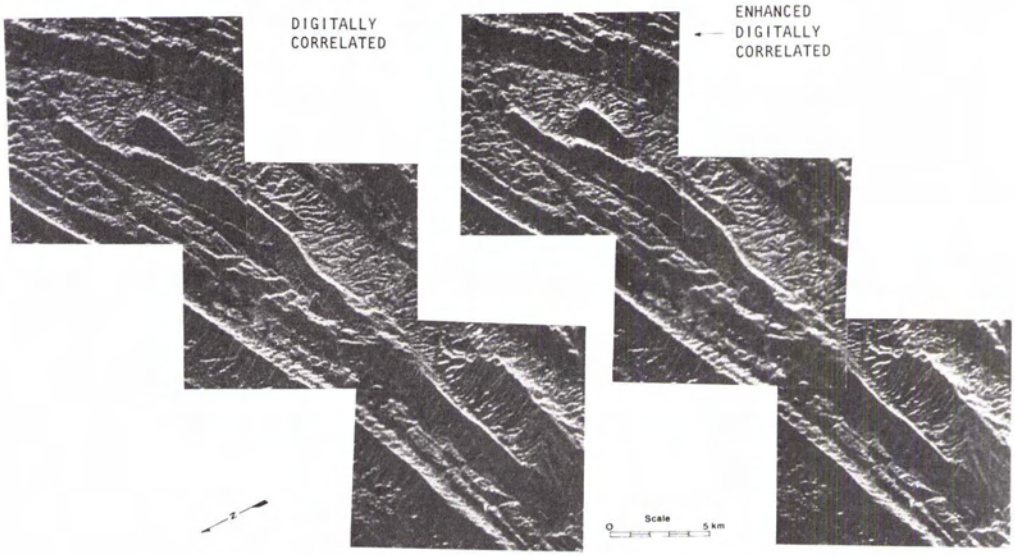

FIG. 6. Pine Mountain enhanced area.

OPTICAL VERSUS DIGITAL CORRELATION

The degree of correlation of imagery derived data with ground truth was dependent on several parameters. A consistent geomorphic expression of a distinct rock type or assemblage of rock types resulted in a high degree of correlation in contrast with a lithology or assemblage of lithologies that lacked consistency in surficial expression. Image reproduction also impaired interpretation.

Not unexpectedly, the lithologic interpretation of the digitally correlated image was more accurate in every respect than the lithologic interpretation of the optically correlated image. The contacts between mapped units corresponded to surficially mapped contacts much more often on the map produced from the digitally correlated image.

The lineament analysis of the digitally correlated image resulted in detection of 54 percent more linears (geological and cultural) than on the

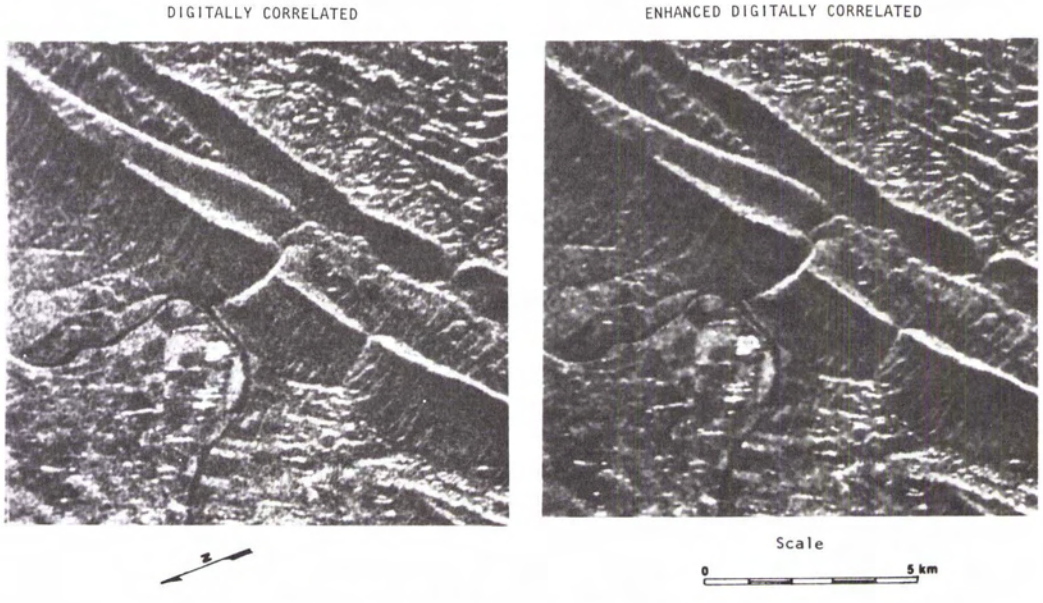

FIG. 7. Church Hill, Tennessee enhanced area.

optically correlated image, although the distribution of the trends on the digitally correlated imagery was not significantly different from distribution on optically correlated images. Fault placement was more accurate, fewer faults were misinterpreted, and more detailed aspects of fault systems were perceived. All images, as anticipated, displayed a significant reduction in the number of lineaments detectable in a thirty-degree arc to both sides of the SAR look direction (N 67.5 W). This is characteristic of any radar system and is not indicative of the actual number of lineaments present in this sixty-degree arc.

Furthermore, the digitally correlated image was much easier to evaluate. Contact and lineament perception required less time and effort. Difficulty in evaluation of the optically processed image could be attributed in a large part to the absence of a consistent tonal range throughout the image and the amount of noise in the image.

ENHANCEMENT VERSUS NON-ENHANCEMENT

The primary value of enhancement is in the interpretive process. The enhancement program was not so much designed to provide an image from which more data could be extracted but to facilitate the extraction of data by visual means. Obviously, image enhancement cannot create new information; however, it can present the image such that it is easier to extract the desired data without sacrificing any of the information content of the original. This enhancement technique appears to succeed in that aspect. Less effort was required to delineate lithologic boundaries, and the edge enhancement feature of the program results in an increase in detectable lineaments while the lithologic mapping accuracy remained constant.

CONCLUSIONS

Through a cursory geologic evaluation of orbital SAR imagery processed by three methods (optically correlated, digitally correlated, and digitally enhanced) over a portion of the southern Appalachians, as expected, digital correlation was demonstrated to result in more accurate definition of geologic features relative to the optical approach. Furthermore, it has been determined that the enhancement technique (Frost *et al.*, 1981) tested on portions of the digitally correlated image resulted in a modest increase in the relative amount of geologic data discernible. However, more importantly, by decreasing noise content and sharpening tonal boundaries, the enhancement program generated an image from which data could be extracted more rapidly and accurately than from the non-enhanced digitally correlated image.

ACKNOWLEDGMENTS

This work was supported by the California Institute of Technology President's Fund, NASA Contract NAS 7-100, and NASA Contract NAS 9-3.

REFERENCES

Bennett, J. R., and I. G. Cummings, 1979. A Digital Processor for the Production of Seasat-Synthetic Aperture Radar Imagery, *SURGE Workshop*, ESRIN, Frascati, Italy, (ESA Reprint SP-154).

Ford, J. P., 1980. Seasat Orbital Radar Imagery for Geologic Mapping: Tennessee-Kentucky-Virginia, *The American Association of Petroleum Geologists Bulletin*, 64(12), pp. 2064-2094.

Franks, L. E., 1969. *Signal Theory*, Prentice-Hall, Inc., Englewood Cliffs, New Jersey.

Frost, V. S., J. A. Stiles, and J. C. Holtzman, 1980. *Radar Image Processing*, RSL Technical Report, RSL TR 420-1, Final Report, Remote Sensing Laboratory, University of Kansas Center for Research, Inc., Lawrence, Kansas, September 1980.

Frost, V. S., J. A. Stiles, K. Sam Shanmugan, J. C. Holtzman, and S. A. Smith, 1981. An Adaptive Filter for Smoothing Noisy Radar Images, *Proceedings of the IEEE*, 69(1), pp. 133-135.

Goodman, J. W., 1968. *Introduction to Fourier Optics*, McGraw-Hill, New York.

———, 1976. Noise in Coherent Optical Processing, in *Optical Information Processing*, Plenum Press, New York.

Habibi, A., 1972. Two-Dimensional Bayesian Estimation of Images, *Proceedings of the IEEE*, 60(7), pp. 878-884.

Hardeman, W. D., *et al.*, 1966. *Geologic Map of Tennessee:* Tennessee Div. Geology, scale 1:250,000.

Harger, R. O., 1970. *Synthetic Aperture Radar System*, Academic Press, New York.

Harris, L. D., and J. M. Kellberg, 1972. *Overburden Related to Type of Bedrock and Engineering Characteristics of the Bedrock, Knox County, Tennessee:* U.S. Geol. Survey Misc. Inv. Map I-767J, scale 1:125,000.

Jenson, H., G. C. Gram, L. J. Porcello, and E. N. Leith, 1977. Side Looking Airborne Radar, *Scientific American*, October 1977.

Kovaly, J. J., 1976. *Synthetic Aperture Radar*, Artech House, Dedham, Massachusetts.

Oppenheim, A. V., and R. W. Schafer, 1975. *Digital Signal Processing*, Prentice-Hall, Inc., Englewood Cliffs, New Jersey.

Perry, M. S., 1980. *Correlation Analysis of SEASAT-SAR in the Southern Appalachians*, Master's Thesis, Geology Department, University of Kansas, Lawrence, Kansas.

Rodgers, J., 1953. Geologic Map of East Tennessee, *Tennessee Div. of Geol.*, Bull. 58, Part II, scale 1:125,000.

Tomiyasu, Kiyo, 1978. Tutorial Review of Synthetic Aperture Radar (SAR) with Application to Imaging of the Ocean Surface, *Proc. IEEE*, 66(5), pp. 563-583.

Wu, C., B. Barkan, B. Huneycutt, C. Leang, and S. Pang, 1981. *An Introduction to the Interim Digital SAR Processor and the Characteristics of the Associated SEASAT SAR Imagery*, JPL Publication 81-26, Pasadena, California.

(Received 17 April 1981; revised and accepted 30 November 1982)